Marine and Petroleum Geology 157 (2023) 106509

Contents lists available at ScienceDirect

Marine and Petroleum Geology

journal homepage: www.elsevier.com/locate/marpetgeo

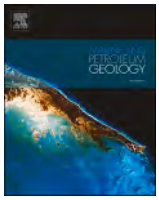

A new age, provenance and tectono-sedimentary setting of the middle Dengying Formation of the terminal Ediacaran in the western Yangtze Block, South China

Zhidong Gu [a,*], Xing Jian [b], Guixia Liu [a]

[a] Research Institute of Petroleum Exploration and Development, PetroChina, Beijing, 100083, China
[b] State Key Laboratory of Marine Environmental Science, College of Ocean and Earth Sciences, Xiamen University, Xiamen, 361102, China

ARTICLE INFO

Keywords:
Zircon U–Pb age
Provenance
Tectono-sedimentary setting
Ediacaran
Dengying Formation
Yangtze Block

ABSTRACT

The widespread terminal Ediacaran Dengying Formation in the western Yangtze Block, South China, is dominated by thick marine dolomite successions deposited in shallow-water platform environments. However, a distinctive succession of mixed clastic and carbonate rocks occurs widely in the middle Dengying Formation, representing sedimentary environment variations. The absolute age of the mixed sedimentary succession is poorly constrained, and tectonic and sedimentary settings remain controversial. In this study, we report a new zircon U–Pb age of 547.3 ± 4.8 Ma from a volcanic ash bed intercalated within a mudstone succession (ca. 40–100 cm thick) in the middle Dengying Formation in the western Yangtze Block. This age is consistent with previously published ages of the middle Dengying Formation or its equivalents in the Yangtze Block and in other blocks worldwide. Field investigations show that the mudstone succession overlies above an unconformity resulted from the lower Dengying Formation weathering and shows a deepening upwards depositional succession representing a period of transgression. Mineralogical analyses show that the mudstones are composed of clay minerals (ca. 68.7%, illite and illite/smectite mixed layers), quartz (24.2%) and minor K-feldspar, indicating a high compositional maturity. Redox sensitive element results (e.g., Mo and U) indicate an increasing anoxic setting upwards. Both elemental geochemical and Lu-Hf-O isotopic analyses suggest that the siliciclastic sediments were moderately weathered (average CIA = 71) and were derived from felsic-intermediate rocks, such as granites and granodiorites (or geochemically-equivalent rocks). We suggest that the mixed sedimentary succession represents as a short-lived, regionally-correlated sea level change event, rather than a tectonic uplift event. Our geochemical data reveal that the mudstone succession accumulated most likely in a passive margin setting, supporting the proposition that the Yangtze Block was located on the periphery of the Gondwana supercontinent during the Ediacaran Period.

1. Introduction

The Ediacaran System spans a remarkable stratigraphic interval in the Earth history between the termination of global Cryogenian glaciation and the beginning of the Cambrian biological radiation (Knoll et al., 2004, 2006). It occurs widely in the Yangtze Block, South China, consisting of the Doushantuo Formation and the overlying Dengying Formation (Zhu et al., 2007; Zhou et al., 2019). The Doushantuo Formation has been well constrained between 635.2 ± 0.6 Ma and 551.1 ± 0.7 Ma from basal and topmost ash beds in the type Yangtze Gorges area (Condon et al., 2005). The base of the Dengying Formation is approximately constrained by accepting the age of the topmost Doushantuo Formation, i.e., 551.1 ± 0.7 Ma (Condon et al., 2005). Furthermore, the boundary of the Ediacaran and Cambrian is recently constrained at 538.8 Ma from ash beds in southern Namibia integrating with biostratigraphic and chemostratigraphic data (Linnemann et al., 2019), more than 2 Myr younger than previously dated age of 541.00 ± 0.81 Ma from the Ara Group in Oman (Bowring et al., 2007). In this case, the Dengying Formation may be regarded to occupy a short-lived duration of ca. 12.3 Ma, between 551.1 ± 0.7 Ma and 538.8 Ma.

The Dengying Formation has received considerable attention due to the development of biostratigraphy, chemostratigraphy, and geochronology in the Yangtze Block (Zhou et al., 2019), and recent discovery of the Anyue gas field in the Sichuan Basin (Zou et al., 2014; Xu et al.,

* Corresponding author.
E-mail address: guzhidong@petrochina.com.cn (Z. Gu).

https://doi.org/10.1016/j.marpetgeo.2023.106509
Received 7 June 2023; Received in revised form 10 September 2023; Accepted 19 September 2023
Available online 20 September 2023

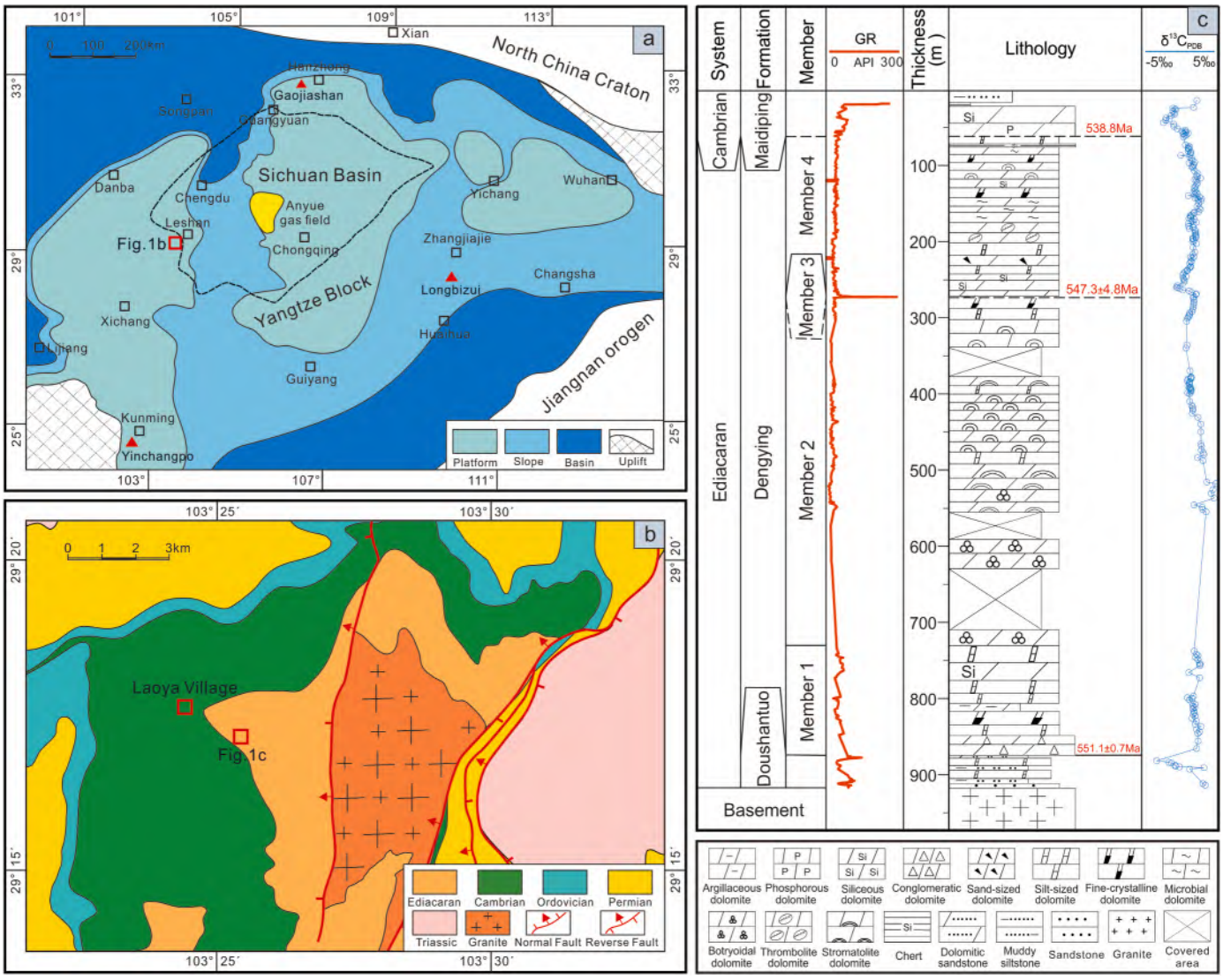

Fig. 1. Simplified paleogeographic map, local geological map and integrated stratigraphic column for the Ediacaran Dengying Formation in the western Yangtze Block, South China. (a) Simplified regional paleogeographic map of the Yangtze Block during the Ediacaran Dengying Formation interval, showing platform, slope and basin facies, respectively. This map also marks the locality of the Sichuan Basin with black dash line, the study site with red square, and the Anyue gas field with yellow polygon. (b) Sketch geological map of the study area showing distribution of Ediacaran-Ordovician strata and the location of the measured Laoya section with red square. (c) Integrated lithostratigraphy, $\delta^{13}C$ chemostratigraphy and geochronology from the Laoya section (547.3 ± 4.8 Ma) corresponding to Fig. 1b, with a basal age (551.1 ± 0.7 Ma, Condon et al., 2005) and a top age (538.8 Ma, Linnemann et al., 2019) for the Dengying Formation. Lithostratigraphic and $\delta^{13}C$ data are modified after Deng et al. (2015).

2020). The Dengying Formation is dominated by thick marine carbonate successions deposited in shallow-water platform environments (Zhu et al., 2003, 2007). However, a distinctive succession of mixed clastic and carbonate rocks occurs widely in the middle Dengying Formation above a regional unconformity, representing sedimentary environment variations. Yang et al. (2017a) reported two SIMS zircon U–Pb ages of 553.6 ± 2.7 Ma and 546.3 ± 2.7 Ma, from ash beds in the Jiucheng Member of the middle Dengying Formation at the Yinchangpo section in eastern Yunan Province. Cui et al. (2016) yielded a LA-ICP-MS zircon U–Pb age of 548 ± 8 Ma for detrital zircons from the Gaojiashan Member of the middle Dengying Formation at the Gaojiashan section in southern Shaanxi Province. Yang et al. (2017b) reported a CA-ID-TIMS zircon U–Pb age of 545.76 ± 0.66 Ma from an ash bed in the Lower Liuchapo Formation in a deep-water setting at the Longbizui section in western Hunan Province.

Furthermore, different viewpoints have been proposed to explain the formation of the mixed sedimentary succession, i.e., tectonic uplift (Cao et al., 1989; Xue et al., 2001; Xing et al., 2015; Feng et al., 2017; Yang et al., 2017b; He et al., 2023), tectonic subsidence increase (Duda et al., 2016), extensional rifting (Wei et al., 2015; Zhou et al., 2017; Zi et al., 2017), and sea-level change (Zhu et al., 2007; Cui et al., 2019; Deng et al., 2020; Gu et al., 2021, 2023). Therefore, the absolute age of the mixed sedimentary succession in the middle Dengying Formation is poorly constrained, and tectonic and sedimentary settings remain controversial.

In this contribution, we performed an integrated study of mineralogy, whole-rock geochemistry, zircon U–Pb dating, and Hf–O isotopic elements for a mudstone succession within the middle Dengying Formation at the Laoya section of Leshan City in the western Yangtze Block. The mudstone succession was systematically sampled, where a volcanic ash bed was collected and dated using the SHRIMP method. Also, mineralogy and elemental geochemistry of mudstone samples were carried out to interpret the paleoweathering and paleoredox conditions, provenance, as well as tectonic and sedimentary settings. This study would throw insights into the geochronological framework of the Dengying Formation and regional tectonic setting during the Ediacaran

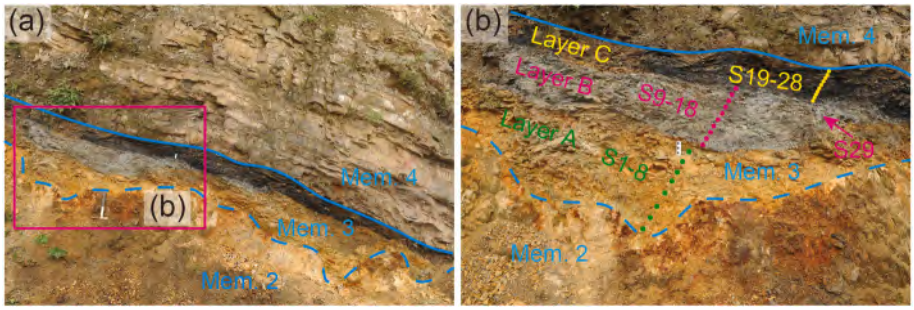

Fig. 2. Field outcrop photographs from the Member 3 of the Ediacaran Dengying Formation at the Laoya section, northeastern Ebian County of Leshan City. (a) The Member 3, consisted of 40–100 cm thick mudstones, overlies unconformably above the Member 2 with a distinct erosional unconformity. The pink square denotes the site in Fig. 2b and the hammer is ca. 30 cm for scale. (b) Enlarged field photo showing the details of the Member 3 and distribution of collected samples. The lithostratigraphic column comprises, from base to top, light grey mudstone (Layer A, Sample GPS808-1~8), dark tuffaceous mudstone (Layer B, Sample GPS808-9~18), and black mudstone (Layer C, Sample GPS808-19~28). Sample GPS808-29 was collected from a volcanic ash bed for zircon U–Pb dating.

Period.

2. Geological setting

The Yangtze Block is located in the northwestern South China Craton, which separates with the Cathaysia Block southeastward by the Jiangnan orogen (Zhao and Cawood, 2012). The Ediacaran was deposited above the glacial tillite of the Cryogenian Nantuo Formation on a passive margin setting (Jiang et al., 2007, 2011; Zhou and Xiao, 2007; Zhou et al., 2018, 2019) following extensive continental rifting during the Neoproterozoic in the Yangtze Block (Wang and Li, 2003; Yang et al., 2017a; Domeier, 2018). Overall, the Ediacaran in the Yangtze Block was deposited in a shallow-water carbonate platform surrounded by deep-water slope-basin deposition (Jiang et al., 2007, 2011; Gu et al., 2021, 2023). The early Ediacaran Doushantuo Formation comprises a succession of carbonate, shale, and phosphatic shale in its type area (Condon, et al., 2005).

The terminal Ediacaran Dengying Formation is dominated by thick carbonate rocks in shallow-water settings, and thin cherts as well as black shales in deep-water settings (Fig. 1a) (Zhu et al., 2003, 2007; Vernhet et al., 2006; Yang et al., 2017b). In the shallow-water platform setting, the Dengying Formation is lithostratigraphically divided into three parts set apart by the middle mixed sedimentary rocks including siliciclastic rocks, volcanic rocks, carbonate rocks and cherts (Zhu et al., 2003; Yang et al., 2017a). The three parts, in ascending order, have been referred to as the Hamajing, Shibantan and Baimatuo members in the Yangtze Gorges area (Zhao et al., 1985; Zhu et al., 2003, 2007; Chen et al., 2014), the Donglongtan, Jiucheng and Baiyangshao members in eastern Yunnan Province (Zhu et al., 2007), and the Algal dolomite, Gaojiashan and Beiwan members in southern Shaanxi Province (Ding et al., 1992; Yang et al., 2017a). The lower and middle parts are separated by a widely erosional unconformity (Zhu et al., 2003, 2007). The other common stratigraphic division involves four members for the Dengying Formation in the Sichuan Basin according to the microbial content and lithostratigraphic features (Yang et al., 2014; Zhou et al., 2016; Hu et al., 2018). In this division, the middle mixed sedimentary rocks are referred to as the Member 3, and the lower and upper parts are called the Members 1–2 and Member 4, respectively (Yang et al., 2014). Abundant fossils have been discovered in the middle Dengying Formation, such as the Gaojiashan biota in southern Shaanxi Province, the Xilingxia biota in the Yangtze Gorges, and the Jiangchuan biota in eastern Yunnan Province (Chen et al., 2014; Yang et al., 2017a; Cui et al., 2019). Thus, the Shibantan Member (Yangtze Gorges), the Gaojiashan Member (South Shaanxi), the Jiucheng Member (East Yunnan) and the Member 3 (Sichuan Basin) of the Dengying Formation can be considered as the isochronous interval.

The Laoya section is located in northeastern Ebian County of Leshan City (Fig. 1b), southwestern Sichuan Province, in the western Yangtze Block. The Dengying Formation (ca. 812-m-thick) at this section is well exposed and was carefully measured (Fig. 1c and Deng et al., 2015). It is composed of four members: Members 1 and 2 (ca. 602-m-thick) are dominated by thick dolomites with an erosional unconformity surface at the top (Fig. 2a); Member 3 (ca. 40–100 cm thick) comprises, from base to top, light grey mudstone (Layer A, ca. 50-cm-thick), dark tuffaceous mudstone (Layer B, ca. 30-cm-thick), and black mudstone (Layer C, ca. 20-cm-thick) (Fig. 2b); Member 4 is dominated by thick dolomites (ca. 210-m-thick), which is unconformably overlain by the Cambrian Maidiping Formation (Fig. 1c).

3. Samples and methods

3.1. Samples

A total of 28 samples were collected from the Member 3 mudstones (ca. 1-m-thick) for major, trace and rare earth element analyses, including 8 samples from Layer A (GPS808-1~808-8), 10 samples from Layer B (GPS808-9~808-18) and 10 samples from Layer C (GPS808-19~808-28) (Fig. 2b). Two samples (GPS808-29-1~808-29-2) were collected from the Layer B for clay X-ray diffraction (XRD) analysis. A volcanic ash-rich sample (GPS808-29) was collected approximately 80 cm above the base of the Member 3 (Fig. 2b) for zircon U–Pb dating and Hf–O isotopic analyses.

3.2. Methods

3.2.1. X-ray diffraction (XRD)

Bulk-rock mineralogical and clay mineralogical compositions were analyzed for selected samples through the X-ray diffraction (XRD) method. The XRD analyses were performed using a D/max-2500 and TTR Power X-ray diffractometer at Key Laboratory of Oil and Gas Reservoirs, PetroChina. For bulk-rock XRD analysis, the samples were first powdered to 200 mesh in an agate mortar and the rock powders were then scanned in the X-ray diffractometer. For clay mineral XRD analysis, loose samples were soaked in deionized water, and then were dispersed using an ultrasonic oscillator. Clay flocculation was avoided by adding sodium hexametaphosphate. The particles <2 μm were separated according to the Stoke's law. The separated clay particles were made to oriented mounts. Air-dried, ethylene glycol-saturated and heated mounts were successively scanned in the X-ray diffractometer. An MDI jade software was used for data smoothing, peak value extraction and phase identification and semi-quantitative compositions were determined. XRD data are listed in Table S1 in the supplementary Appendix A.

3.2.2. Major, trace and rare earth element analyses

Whole-rock major and trace elements were analyzed by using an X-ray fluorescence spectrometer (XRF) and an Inductively Coupled Plasma Mass Spectrometer (ICP-MS), respectively, at the Analytical Laboratory, Beijing Research Institute of Uranium Geology. The Loss on ignition (LOI) data were obtained through measuring weight loss after heating

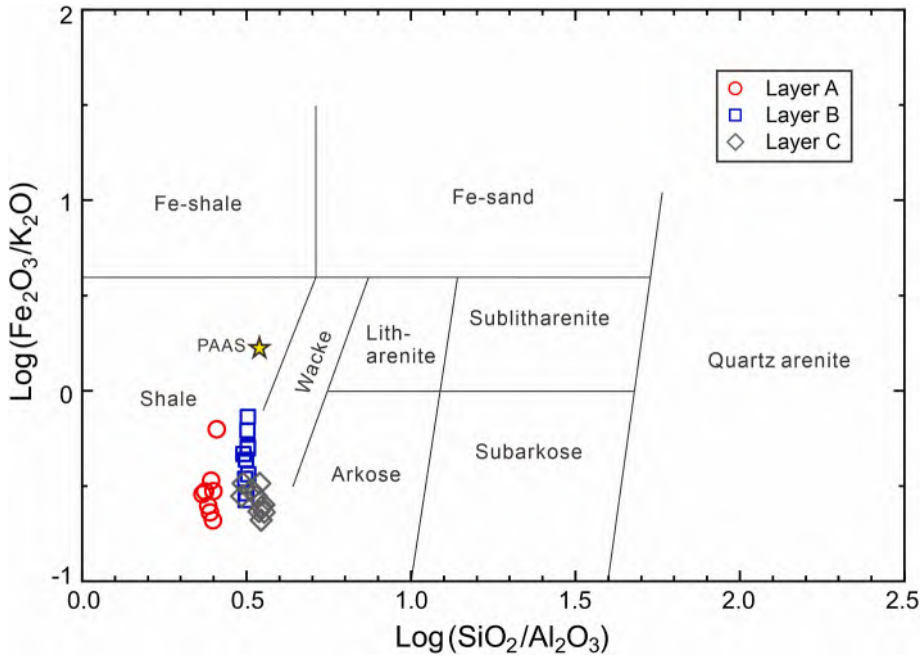

Fig. 3. Chemical classification diagram for discriminating siliciclastic sediments by their logarithmic ratios of SiO_2/Al_2O_3 vs. Fe_2O_3/K_2O after Herron (1988). The Post-Archean Australian Shale (PAAS) data are from Taylor and McLennan (1985).

sample powders at 980 °C. Major element compositions were obtained based on well-mixed glass disks which were made by high-temperature fusion of samples powders and lithium metaborate flux. Sample powders were completely dissolved by Hf–HNO_3–$HClO_4$ mixture acid solutions and diluted with 1% HNO_3 for trace and rare earth element determination. Detailed methods were described by Gu et al. (2023). Whole-rock major, trace and rare earth element analyses are listed in Tables S2–S3 in the supplementary Appendix A.

3.2.3. Zircon separation and CL imaging

Zircon grains were separated from concentrates of the sample processed by conventional magnetic and density techniques. The zircon grains, together with the zircon standard TEMORA (reference age of 417 Ma), were mounted in an epoxy-resin mount, which was then polished until the crystal interiors were exposed. All zircons were documented with transmitted and reflected light micrographs as well as cathodoluminescence (CL) images to reveal their internal structures, and the mount was vacuum-coated with gold for SHRIMP analysis (Zhou et al., 2018).

3.2.4. Zircon U–Pb–O isotopic analyses

Zircon U–Pb–O isotopic analyses were performed using the SHRIMP Ⅱ at the Beijing SHRIMP Center, Institute of Geology, Chinese Academy of Geological Sciences, following procedures described by Compston et al. (1992). U–Th–Pb isotopic ratios were determined relative to the TEMORA standard zircon with $^{206}Pb/^{238}U = 0.0668$ corresponding to 417 Ma, and the absolute abundances were calibrated to the standard zircon SL13 (Ye et al., 2007). The data were processed using the Squid v. 1.02 and Isoplot/Ex v. 2.49 programs, and common Pb was corrected against measured ^{204}Pb. Uncertainties in ages are reported at 1σ level, and the weighted mean ages are quoted at 95% confidence level. Detailed methods were described by Gu et al. (2014), Zhou et al. (2018) and Li et al. (2021). For the O isotopic compositions of the dated zircons, analyses of in-house zircon standard TEMORA-2 ($\delta^{18}O_{VSMOW} = +8.20 \pm 0.02‰$; Black et al., 2004) embedded in each epoxy mount are interspersed with every three or four unknown sample measurements.

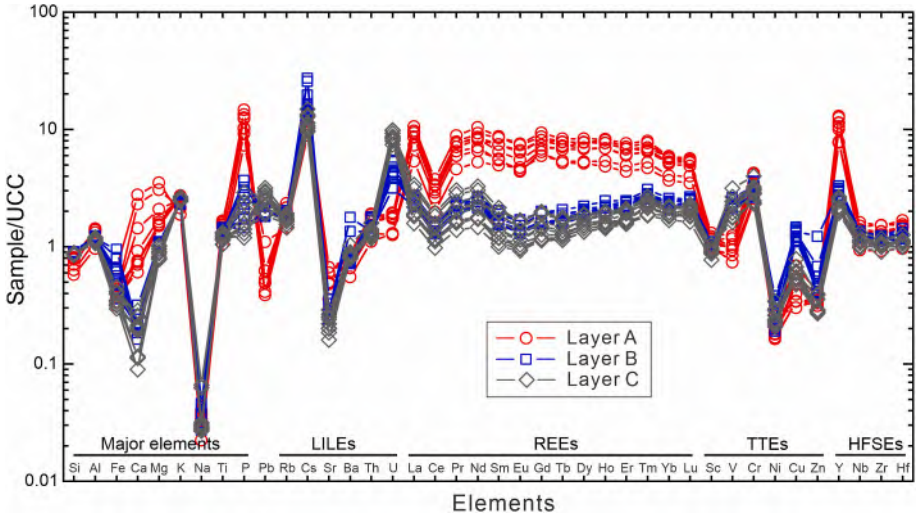

Fig. 4. Major and trace element geochemical results of all the analyzed samples. All the element data were normalized by the Upper Continental Crust (UCC) compositions. The UCC data are from Rudnick and Gao (2014). LILEs: large ion lithophile elements; REEs: rare earth elements; TTEs: transition trace elements; HFSEs: high field strength elements. Note that the Layer A samples are comparatively rich in Ca, Mg, P, Y and REEs, whereas the Layers B–C samples are rich in Pb, U and V.

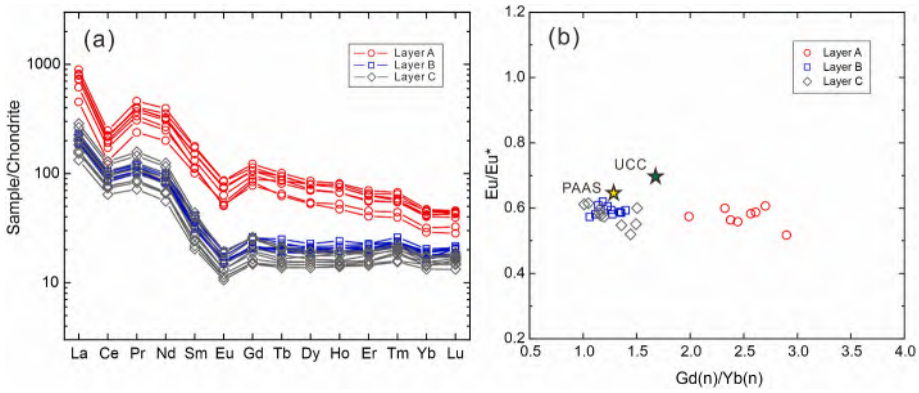

Fig. 5. (a) Chondrite-normalized REE patterns of the analyzed samples. (b) Binary plots between Eu/Eu* (Eu anomaly values) and $Gd_{(n)}/Yb_{(n)}$ ratios (chondrite-normalized element ratios). The data of chondrite, UCC and PAAS are from McDonough and Sun (1995), Rudnick and Gao (2014), and Taylor and McLennan (1985), respectively. The results show that the Layer A samples indicate enrichment of REEs and obviously negative Ce anomalies.

Analytical uncertainties of each unknown sample analysis combine the internal run errors (s.e., typically 0.1–0.4‰) and the reproducibility of the standard zircon analyses (2 s.d. after the instrumental drift correction). $\delta^{18}O$ data are corrected to VSMOW via the UWG-2 standard. Zircon U–Pb and O isotopic data are given in Tables S4 and S5 in the supplementary Appendix A.

3.2.5. Zircon Lu–Hf isotopic analyses

After U–Pb dating, zircon Lu–Hf isotopic analyses was performed using a GeoLas 193 nm laser ablation system attached to a Neptune (Plus) MC-ICP-MS at MiDeR-NJU. Standard zircon Mud Tank ($^{176}Hf/^{177}Hf = 0.282507 \pm 6$; Woodhead and Hergt, 2005) and 91500 were used to monitor accuracy and precision of Hf isotopic ratios with respect to the Lu/Hf ratios. The measured $^{176}Hf/^{177}Hf$ ratios and ^{176}Lu decay constant of 1.867×10^{-11} $year^{-1}$ were used to calculate initial $^{176}Hf/^{177}Hf$ ratios. The chondritic values of $^{176}Lu/^{177}Hf = 0.0336 \pm 1$ and $^{176}Hf/^{177}Hf = 0.282785 \pm 11$ (2σ) were used for calculations of εHf values. Detailed methods were described by Li et al. (2018, 2021). Zircon Lu–Hf isotopic data are given in Table S6 in the supplementary Appendix A.

4. Results

4.1. Mineral compositions

The bulk-rock XRD analysis results indicate that the Layer B samples are composed of clay minerals (64.8%–72.6%) and quartz (23.1%–25.3%), with subordinate K-feldspar, pyrite and gypsum. The clay minerals therein are predominated by illite and illite/smectite mixed layers.

4.2. Major, trace and rare earth elements

All the analyzed samples have relatively high Al and K and low Si and Fe contents. In the binary diagram of Log (SiO_2/Al_2O_3) and Log (Fe_2O_3/K_2O), the Layer A samples fall into the "shale" field, whereas the Layers B and C samples fall into the fields close to "Wacke" (Fig. 3). Samples from the Layer A indicate comparatively higher abundances of Ca and P than those from the Layers B and C and all the samples show depletion in Na relative to Upper Continental Crust (UCC) compositions (Fig. 4). Furthermore, all the samples are depleted in Sr but are rich in Cs. The samples from Layers B and C indicate relative enrichment of U and V, whereas the samples from Layer A display comparative enrichment of rare earth elements (REEs) and Y (Fig. 4). The REEs concentrations were normalized to the standard chondrite compositions (Fig. 5a) and the results indicate that all the samples have clear patterns of light REEs enrichment and negative Ce and Eu anomalies. Samples from the Layers B and C show fairly uniform REE patterns with relatively flat heavy REEs, whereas Layer A samples have higher total concentrations of REEs (most ranging 600–1100 ppm, Fig. 6a) and higher $Gd_{(n)}/Yb_{(n)}$ ratios (chondrite-normalized rare earth element ratios, most >2.0, Fig. 5b).

4.3. Zircon U–Pb ages

Most of the analyzed zircon grains are euhedral and prismatic in morphology, and 100–300 μm in length with aspect ratios from 2 to 4.

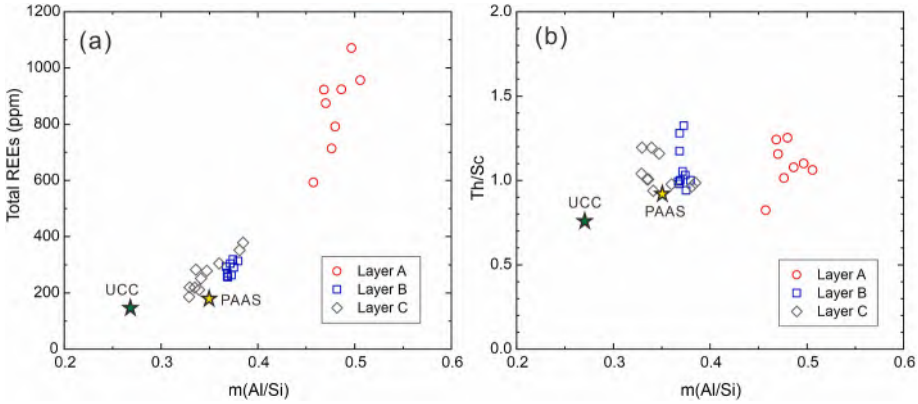

Fig. 6. Binary diagrams between concentrations of REEs and Al/Si (a), Th/Sc and Al/Si (b). The enrichment of REEs in the Layer A samples is due to relatively high clay mineral compositions. All the samples have similar Th/Sc ratio values, implying similar parent-rock compositions (i.e., dominated by felsic rocks). The UCC and PAAS data are from Rudnick and Gao (2014), and Taylor and McLennan (1985), respectively.

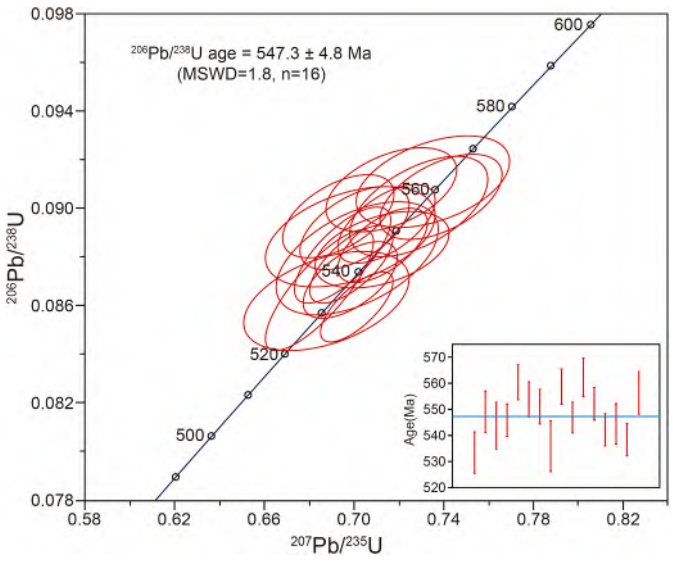

Fig. 7. SHRIMP zircon U–Pb concordia plot with a weighted mean $^{206}Pb/^{238}U$ age of 547.3 ± 4.8 Ma (MSWD = 1.8, n = 17) at 95% confidence level from sample GPS808-29 collected in a volcanic ash bed. Ellipse and error line of data points represent 2σ uncertainty. MSWD-mean square weighted deviation.

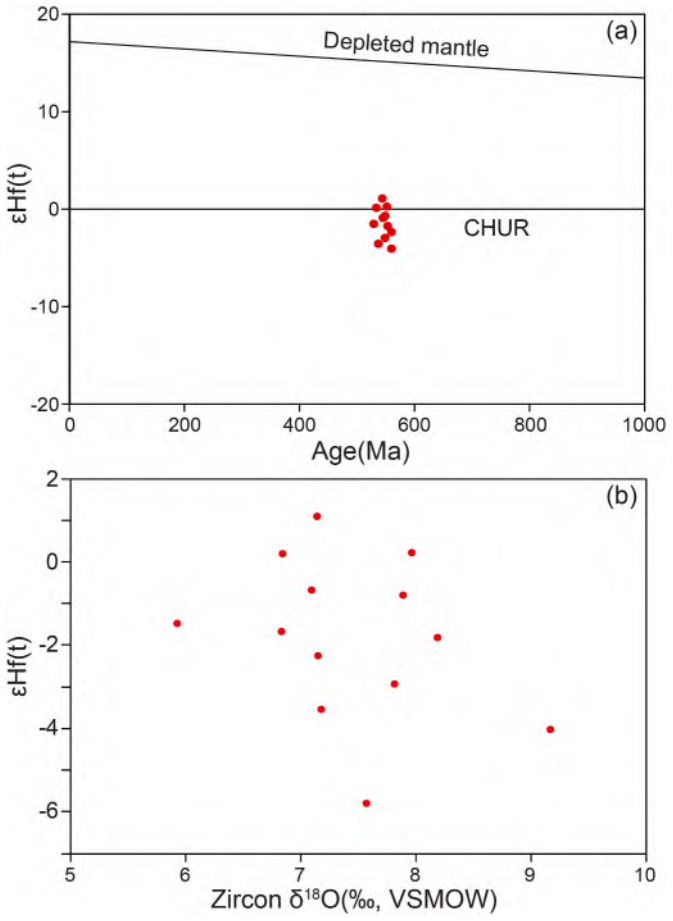

Fig. 8. The ƐHf (t)-Age and ƐHf (t)-$\delta^{18}O$ plots showing continent-derived source features. (a) The ƐHf values plotted against age (Ma). Grains with discordant ages have been omitted. DM-depleted mantle, CHUR-chondritic uniform reservoir. (b) The ƐHf (t)- $\delta^{18}O$ (‰, VSMOW) values with concordant ages.

Most zircon grains show oscillatory zoning according to CL images. A total of 27 spots were conducted on 27 zircon grains. Except 4 sets of data with high U content (704–1361 ppm), a datum with high $^{232}Th/^{238}U$ ratio (0.95), and 6 data with larger discordant, others are considered to be reliable. U and Th contents of the remaining 16 data are between 96 and 537 ppm, 55 and 279 ppm, respectively, with Th/U ratios of 0.39–0.77, suggestive of magmatic origin. The age calculation was based on these 16 grains, and their $^{206}Pb/^{238}U$ ages range from 533 ± 8 Ma to 560 ± 6.7 Ma, yielding a weighted mean $^{206}Pb/^{238}U$ age of 547.3 ± 4.8 Ma (1σ, n = 16, MSWD = 1.8) (Fig. 7). This mean age is interpreted to be the crystallization age of the zircons and is also the best estimate of the deposition age for the Member 3 in the middle Dengying Formation.

4.4. Zircon O and Hf isotopic results

O and Hf isotopic data were collected from dated zircon grains of the sample GPS808-29 with concordant ages in order to determine the provenance of the volcanic zircon grains. A total of 11 spots were analyzed for Hf isotopes, and yielded the εHf(t) values between −4.03 and 1.09, with a mean value of −1.44 (Fig. 8a). A total of 13 spots were analyzed for $\delta^{18}O$ isotopes, and yielded the values between 6.83‰ and 9.17‰, with a mean value of 7.63‰ (Fig. 8b).

5. Discussion

5.1. Stratigraphic correlation for the middle Dengying Formation

Since the discovery of the Anyue giant gas field in the central Sichuan Basin in 2011, stratigraphic studies of the Dengying Formation have gained significant advancement (Deng et al., 2015; Gu et al., 2023). Due to the distinct features and widespread occurrence of mixed sedimentary rocks within the middle of thick carbonate successions in the Ediacaran Dengying Formation, the mixed sedimentary record has been widely used for stratigraphic subdivision and correlation for the Dengying Formation in the Yangtze Block, South China. In terms of datable volcanic ash beds intercalated sparsely within the mixed succession, some researchers attempted to gain depositional ages for the Laoya section using different methods. For example, Deng et al. (2015) first published a zircon U–Pb age of 543 ± 12 Ma with the SHRIMP method, but they did not provide the details related to the age. In addition, the age error of 12 Ma is much larger than a standard age error (one percent for an Ediacaran age, ca. 5 Ma). Moreover, Zi et al. (2017) provided a zircon U–Pb age of 539.6 ± 1.4 Ma from the same ash bed using the LA-ICP-MS method, which was thought to correlate with the Ediacaran-Cambrian boundary age (ca. 541 ± 1 Ma) in the Yangtze Block. However, we note that the lithostratigraphic succession (ca. 200-m-thick) above the Member 3 mixed succession has unique characteristics of the Dengying Member 4, and the Ediacaran Dengying Formation and Cambrian Maidiping Formation boundary can be readily recognized (Fig. 1c). Hence, if the mixed succession in the middle Dengying Formation is considered as the Ediacaran-Cambrian boundary, the ca. 200-m-thick dolomites of the Dengying Member 4 would be absent, which is inconsistent with the lithostratigrapic framework in the vicinity of the Sichuan Basin. In this study, the newly obtained age of 547.3 ± 4.8 Ma is between the recalibrated Dengying Formation age ranges (ca. 551.1 ± 0.7 Ma to ca. 538.8 Ma), which is a reliable and precise age from the point of data qualities and lithostratigraphic successions.

On the other hand, the age of 547.3 ± 4.8 Ma obtained in this study is consistent with other ages reported for the Yangtze Block and locations around the world (Fig. 9). A few radiometric ages from the middle Dengying Formation or its equivalents in the Yangtze Block have been reported. For instance, Yang et al. (2017a) reported a SIMS zircon U–Pb age of 546.3 ± 2.7 Ma from an ash bed in the middle Jiucheng Member in eastern Yunnan Province. Moreover, Yang et al. (2017b) provided a CA-ID-TIMS zircon U–Pb age of 545.76 ± 0.66 Ma from an ash bed of the

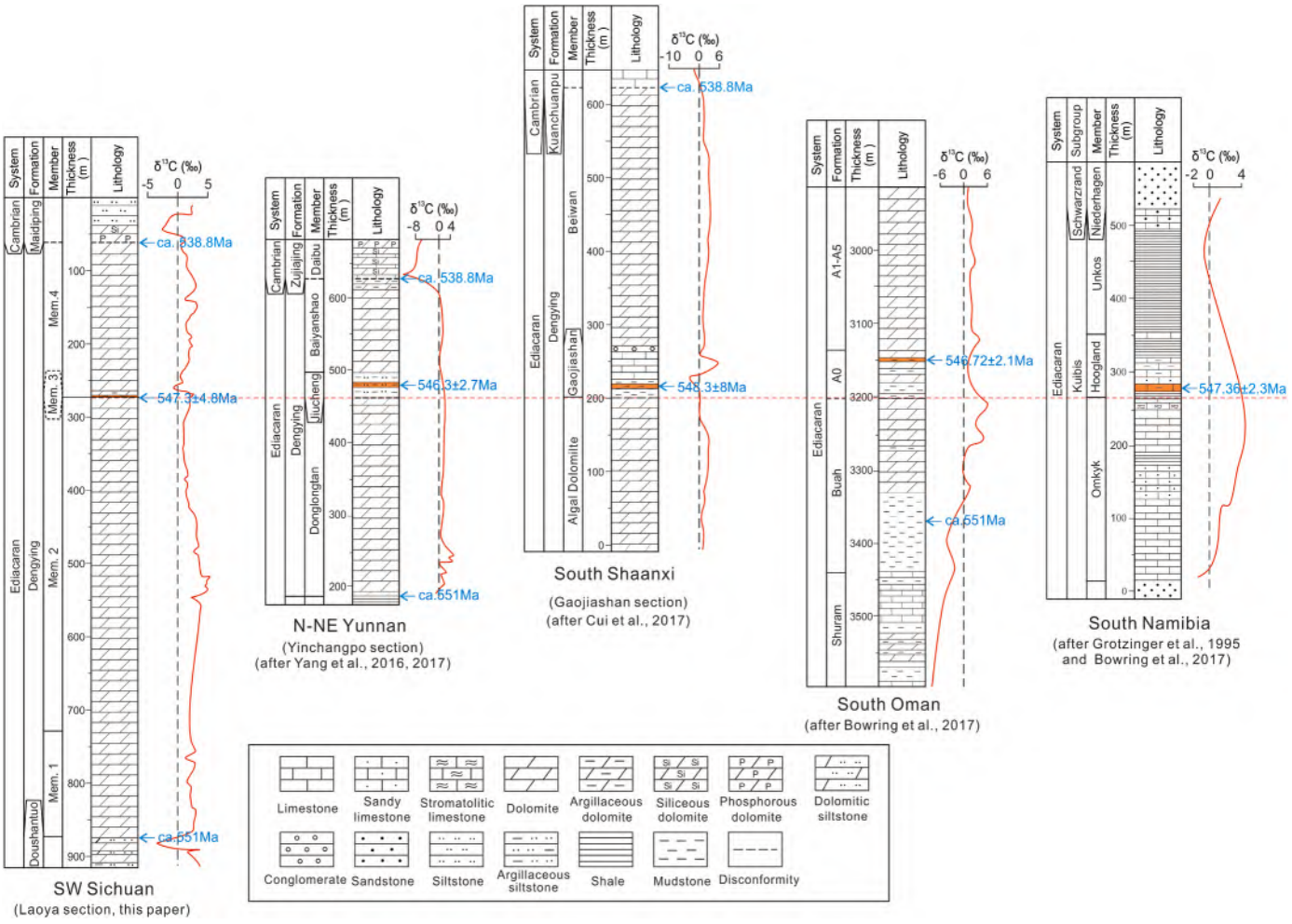

Fig. 9. Stratigraphic correlation of the middle Dengying Formation and its equivalents in the Yangtze Block, Oman as well as Namibia constrained by both U–Pb ages and carbon isotopic data. The age of 547.3 ± 4.8 Ma in southwestern Sichuan (this paper) is consistent with the age of 546.3 ± 2.7 Ma (Yang et al., 2017a) in eastern Yunnan, the maximum depositional age of 548.3 ± 8 Ma (Cui et al., 2016) in southern Shaanxi, and is also identical to the age of 547.36 ± 0.23 Ma in Namibia and the age of 546.72 ± 0.21 Ma in Oman (Bowring et al., 2007). The $\delta^{13}C$ curve presents similar trend from slightly positive to minorly negative values across the Member 3 of the middle Dengying Formation and its equivalents worldwide. See Fig. 1a for locations.

Lower Liuchapo Formation in a deep-water setting in western Hunan Province. Cui et al. (2016) yielded a LA-ICP-MS zircon U–Pb age of 548 ± 8 Ma from detrital zircons in the Gaojiashan Member in southern Shaanxi Province to constrain the maximum depositional age. From the ordinal relationship of these ages, the age of 547.3 ± 4.8 Ma in southwestern Sichuan denotes the base of the middle Dengying Formation, the age of 546.3 ± 2.7 Ma from eastern Yunnan (Yang et al., 2017a) indicates the middle of the mixed sedimentary succession, and the age of 545.76 ± 0.66 Ma from western Hunan (Yang et al., 2017b) may represent the top of the middle Dengying Formation. These age results are consistent with the sample localities in the stratigraphic successions from the middle Dengying Formation. Taking into account synchronous ages worldwide, Grotzinger et al. (1995) reported a zircon U–Pb age of 548.8 ± 0.23 Ma from an ash bed in the Hoogland Member of the Kuibis Subgroup, Nama Group, in southern Namibia, which was further refined to 547.36 ± 0.23 Ma by Bowring et al. (2007) using the CA-TIMS method. In addition, Bowring et al. (2007) reported a U–Pb age of 546.72 ± 0.21 Ma from an ash bed in the lowermost Ara Group, Sultanate of Oman. Similarly, there is also an unconformity occurred between the Ara Group and underlying the Buah Formation (Bowring et al., 2007). Thus, the ages (547.3 ± 4.8 Ma, 546.3 ± 2.7 Ma) for the middle Dengying Formation in the Yangtze Block, South China, is identical to the age (547.36 ± 0.23 Ma) in Namibia and the age (546.72 ± 0.21 Ma) in Oman (Fig. 9), providing a tie-point for the stratigraphic correlation between South China, Oman and Namibia.

The carbon isotopic record from the Ediacaran has been proven to be effective in constraining and correlating the Ediacaran stratigraphy (Jiang et al., 2007; Zhu et al., 2007; Zhou et al., 2019). The $\delta^{13}C$ curve of the Dengying Formation at the Laoya section (Deng et al., 2015, Fig. 1c) shows overall positive values between two distinct $\delta^{13}C$ negative excursions, i.e., the DOUNCE at the topmost Doushantuo Formation and the BACE at the lowermost Cambrian, respectively. However, there is a $\delta^{13}C$ variation from a slightly positive to minorly negative shift occurred close to the Dengying Member 3. The $\delta^{13}C$ values increase upward monotonically from about 0.863‰, approximately 33 m below the Member 3, to a peak of nearly +2.148‰, about 3 m above the Member 3; values then decrease continuously to about −0.473‰, approximately 14 m above the Member 3. Upward at this section, $\delta^{13}C$ values remain positive through the Member 4 with a variation from an increase to a decrease. Furthermore, this $\delta^{13}C$ variation correlates well with other regions in the Yangtze Block and other continents worldwide (Fig. 9). For example, Cui et al. (2019) reported $\delta^{13}C$ data with a positive excursion from the Gaojiashan Member in southern Shaanxi Province; the $\delta^{13}C$ curve from the Kuibis Subgroup in Namibia also shows a positive excursion and the age of 547.36 ± 0.23 Ma occurs in the falling limb of the positive excursion (Bowring et al., 2007); the $\delta^{13}C$ curve from the Ara Group in Oman presents a similar variation trend with the age of 546.72 ± 0.21 Ma occurred just above the zero crossing after the

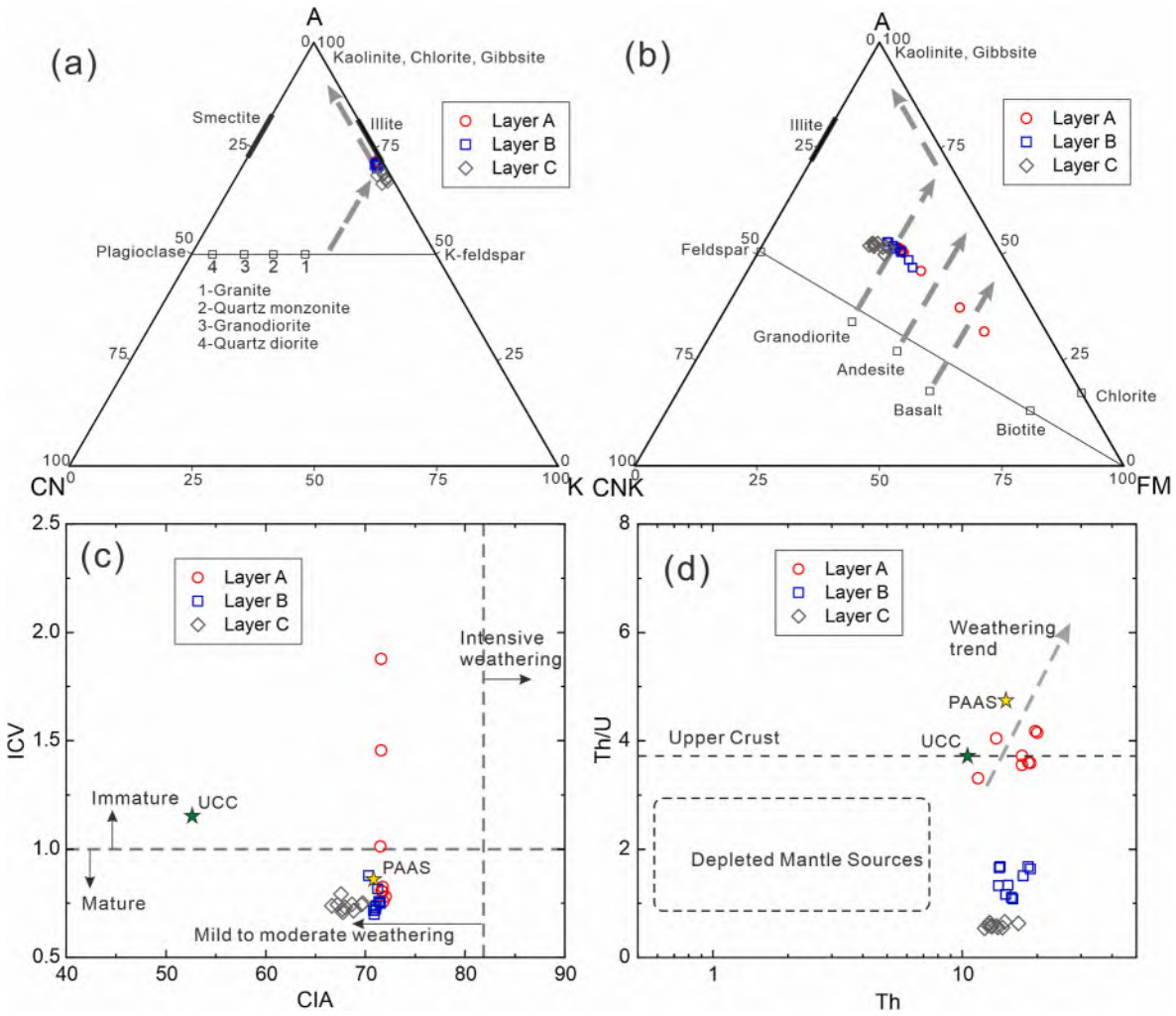

Fig. 10. Weathering intensity and maturity analysis results of the analyzed samples. (a) A–CN–K ternary diagram (modified from Fu et al. (2022)); (b) A-CNK-FM ternary diagram (modified from McLennan et al. (1993)); (c) binary plots between ICV and CIA values; (d) binary plots between Th/U and Th concentration (modified from McLennan et al. (1993)). The UCC and PAAS data are from Rudnick and Gao (2014), and Taylor and McLennan (1985), respectively. Note that most of these samples are mature and moderately weathered from felsic parent-rocks. The low Th/U ratios of samples from the Layers B and C are due to U enrichment, rather than supply from mafic parent-rocks. The chemical weathering intensity classification based on CIA values is from Jian et al. (2013). CIA = $Al_2O_3/(Al_2O_3 + K_2O + Na_2O + CaO) \times 100$ (In the CIA calculation, all variables represent the molar amounts of major-element oxide, and the CaO represents its fraction in silicate minerals only without contributions of CaO from carbonate and phosphate minerals); ICV=$(Fe_2O_3 + K_2O + Na_2O + CaO + MgO + MnO + TiO_2)/Al_2O_3$.

end of the positive excursion (Bowring et al., 2007). In this study, the age of 547.3 ± 4.8 Ma just occurs below the positive $\delta^{13}C$ excursion (Fig. 9). All these results demonstrate that the carbon isotopic variation from slightly positive shift to minorly negative shift took place on the scale of ca.1 Myr or less.

Consequently, the $\delta^{13}C$ isotopic excursion in the middle Dengying Formation and its equivalents between South China, Oman and Namibia can be well correlated. These consistent geochronological results and chemostratigraphic trends indicate that the Late Neoproterozoic $\delta^{13}C$ fluctuations might represent globally synchronous variations in seawater chemistry. Besides, the extensive occurrence of thin volcanic ash beds interbedded within the mixed sedimentary succession reveals a minor volcanic event in the Yangtze Block. Based on the $\delta^{18}O$ and $\epsilon Hf(t)$ results from the dated volcanic zircon grains (Fig. 8), it might be speculated that the volcanic ash was derived from continent, and the origin needs further investigations.

5.2. Maturity, paleoweathering and paleoredox conditions

To better understand the formation environment and accumulation process of the Member 3 mixed sedimentary rocks, here compositional maturity, paleoweathering and paleoredox conditions are interpreted based on the high-resolution major and trace element data. The compositional maturity and chemical weathering intensity of these analyzed samples are indicated using the Index of Compositional Variability (ICV; Cox et al., 1995) and the Chemical Index of Alteration (CIA; Nesbitt and Young, 1982), respectively. Representative redox-sensitive metal elements, such as Mo and U, are employed as indicators for paleoredox environments.

The results indicate that all the Layer B tuffaceous mudstone and Layer C black mudstone samples are compositionally mature, whereas the Layer A shows quite variable maturity (ICV ranging 0.5–2, Fig. 10c). The ICV data support our interpretation that the Layer A of the Member 3 at the investigated outcrop is composed of paleosoils, as a part of paleoweathering section, rather than mature siliciclastic sedimentary rocks. This is also reinforced by the high REEs concentrations (Fig. 5a) which might be due to the weathering of the underlying carbonate rocks. Several case studies on modern carbonate rock weathering and pedogenesis demonstrates that enrichment of REEs is a common phenomenon attributed to clay mineral and REEs-rich phosphate mineral residues (Song et al., 2006; Xu and Han, 2009; Chen and Yang, 2010). This inference is also proven by the high correlations between REEs and Al/Si

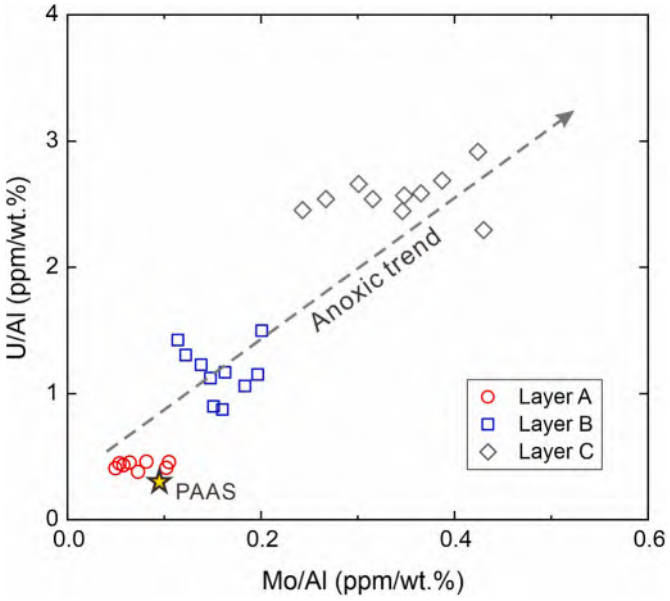

Fig. 11. Representative redox-sensitive metal proxy data of the analyzed samples. Both Mo/Al and U/Al ratios indicate the Layer C was deposited under relatively anoxic environments. The PAAS data are from Taylor and McLennan (1985).

ratios (Fig. 6a) and high P_2O_5 concentrations (Fig. 4).

Both geochemical indicators and mineralogical analysis data demonstrate that the paleosoil and overlying fine-grain sedimentary rocks experienced moderate weathering (Fig. 10c) and were in the initial stage of K-feldspar weathering (Fig. 10a). This implies that the study area was most likely under relatively temperate climate (tend to be warm and humid) conditions during the formation duration of the Member 3. Note that although Th/U ratios to some extent may indicate weathering degrees (McLennan et al., 1993; Carpentier et al., 2013), here the fairly low Th/U ratios for the Layers B and C mudstones (Fig. 10d) are due to anoxia-related U enrichment, rather than mild weathering intensity. Our new results are consistent with previous paleoclimatic analyses on the terminal Ediacaran South China based on lithofacies and geochemical interpretations of the Dengying Formation (e.g., Zhai et al., 2018; Xiao et al., 2020; Lan et al., 2022), which favor a warm and humid climate for the region at that time.

The low Mo and U concentrations in the Layer A paleosoils and comparatively high Mo and U concentrations in the overlying mudstones (Fig. 11) reveal sharp changes in sedimentary environments for the Member 3. We favor that the Layers B and C deposits accumulated under relatively anoxic, deep-water conditions. The anoxia conditions have been widely recognized for the Member 3 in the western Yangtze block (e.g., Cui et al., 2019; Jin et al., 2021). The deep-water sedimentary environments may be attributed to regional transgression or local climate fluctuations. Previous studies also proposed that both significant sea-level rise and warm-humid climate facilitated accumulation of the siliciclastic deposits during that time (Lan et al., 2022).

5.3. Provenance

Multiple geochemical proxies are applied to interpret provenance for the Member 3 siliciclastic deposits (Fig. 12). All the trace and rare earth elements-based binary and ternary plot results indicate that the Layers B and C are composed of PAAS-like sediments (Fig. 5b) and these sediments were derived from source terranes with dominant felsic rocks. Continent-sourced felsic signatures are also reinforced by the major element data. Both the A–CN–K and A-CNK-FM ternary plots (Fig. 10a and b) reveal that parent-rocks are dominated by granite, granodiorite or geochemically-equivalent rocks. Furthermore, although the redox conditions show certain variations between the Layer B tuffaceous mudstone and Layer C black mudstone (Fig. 11), their parent-rocks (Fig. 12) and element-inferred source tectonic setting (Fig. 13) are seemingly indistinguishable. Furthermore, the binary plots of εHf(t)-Age and εHf(t)-$\delta^{18}O$ indicate that the volcanic ash materials were derived from continent sources (Fig. 8). Since paleocurrent and other provenance indicator data (such as detrital zircon U–Pb ages) are not available for this outcrop, we cannot determine specific source terranes for the Member 3 sediments. The Zr/Sc ratios display these sediments did not experience evident recycling (Fig. 12d). According to previous paleogeographical studies and relevant illustrated configurations (e.g., Fig. 1; Qi et al., 2018; Liu et al., 2021; Lan et al., 2022), we infer that the source terranes for the analyzed siliciclastic sediments were nearby paleocontinents to the west, rather than the distant cratons (e.g., India, Australia and Antarctic; Cawood et al., 2018) in the supercontinent Gondwana.

5.4. Tectonic and sedimentary settings

The Ediacaran comprised an essential transitional period from the Neoproterozoic to the Paleozoic times (Knoll et al., 2004), when global tectonic and sedimentary environments also experienced a significant transition from the Rodinia supercontinent cycle to the Gondwana supercontinent cycle (Dalziel, 1997; Merdith et al., 2017; Cawood et al., 2018). Although different paleogeographic positions for the South China Craton during the Ediacaran Period have been proposed by previous investigators, there is a general agreement that it was located in the northern margin of Gondwana facing to the Proto-Tethys Ocean, close to the Australia continent (Yang et al., 2004; Jing et al., 2015) or the India continent (Jiang et al., 2003; Cocks and Torsvik, 2013; Yao et al., 2014). In other words, the western Yangtze Block was adjacent to the Proto-Tethys Ocean during the Ediacaran. Furthermore, lithostratigraphically the Ediacaran ca. 800–1500 m thick carbonate-dominated successions and absence of major tectonic events and intermediate to intense igneous activities collectively favored a view that the Ediacaran (including the Doushantuo and Dengying Formations) was generally deposited in a passive margin setting in the western Yangtze Block (Jiang et al., 2007, 2011; Zhou and Xiao, 2007; Gamper et al., 2015; Yang et al., 2017b; Zhou et al., 2018, 2019; Gu et al., 2021), and it formed an extensive shallow-water carbonate-dominated platform throughout the western Yangtze Block (Chen, et al., 2014; Jiang et al., 2007; Gu et al., 2021, 2023, Fig. 1a). Considering the Ediacaran platform in the Yangtze Block, Gu et al. (2023) suggested that it experienced a sedimentary evolution from a mixed carbonate-siliciclastic ramp of the Doushantuo Formation to a rimmed carbonate platform of the Dengying Formation. Also, the Ediacaran lithostratigraphic successions at the Laoya section effectively support the above suggestions.

To determine the tectonic setting of fine-grained siliciclastic sedimentary rocks, some geochemical indicators, REE patterns, and discriminating diagrams based on major, trace and rare earth elements have been proposed (e.g., Roser and Korsch, 1986, 1988; Nesbitt et al., 1997; Roser, 2000). In the A–CN–K diagram, all of the mudstone samples have similar ratios and cluster tightly on the A-K axis, probably indicating steady state conditions of sources without evident tectonic uplift (Nesbitt et al., 1997; Roser, 2000). The overall chondrite-normalized REE pattern, including LREE enrichment, flat HREE, the accordant negative Eu-anomaly and similar to PAAS, is an indicative of sediments deposited in a passive margin setting (McLennan, 1989). Additionally, on the major element discriminant diagrams of K_2O/Na_2O–SiO_2 and SiO_2/Al_2O_3–K_2O/Na_2O (Fig. 13a and b), all mudstone samples fall into the field of passive margin. Similarly, in the trace element ternary diagram of Th–Co–Zr/10, most of the studied mudstones occupy the passive margin field (Fig. 13c). These geochemical results are also coincident with regional tectonic setting analyses as depicted above.

The Dengying Formation at the Laoya section represents typical sedimentary features within the western Yangtze Block, i.e., the middle

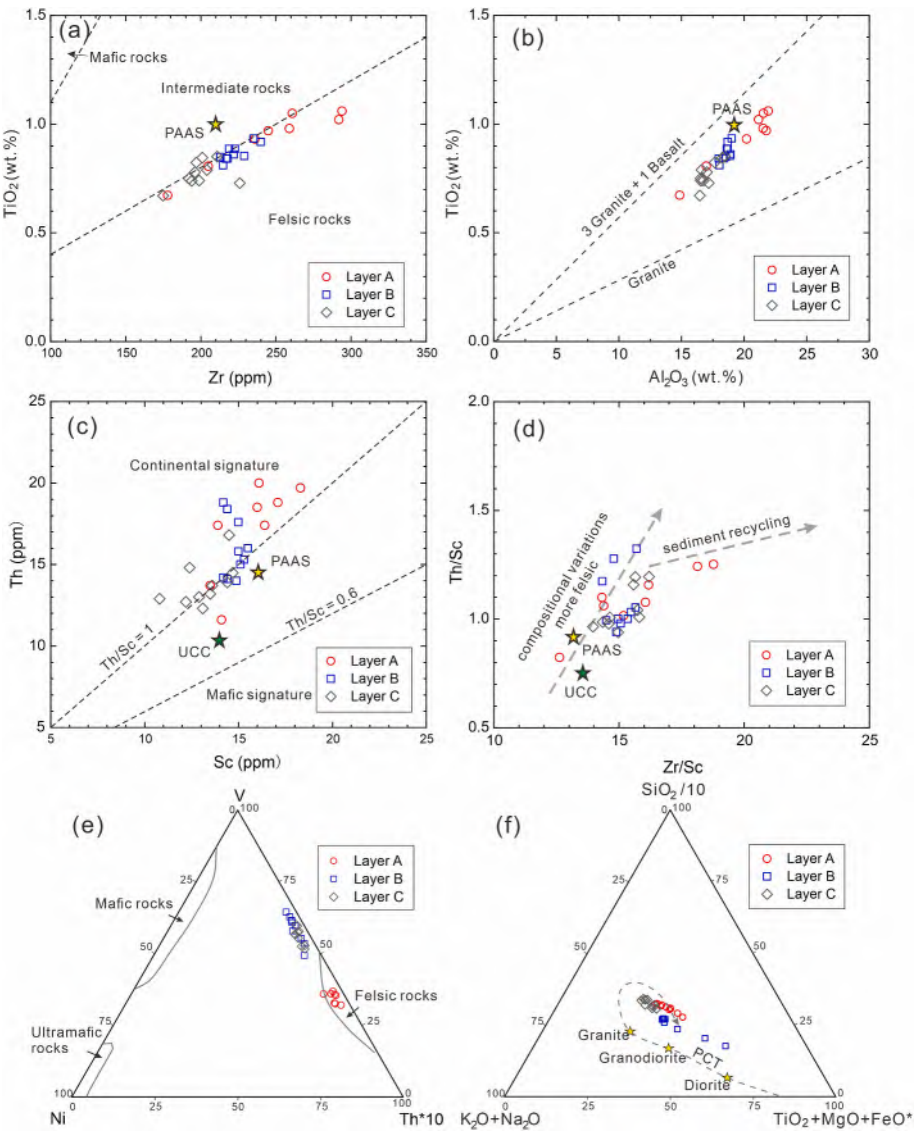

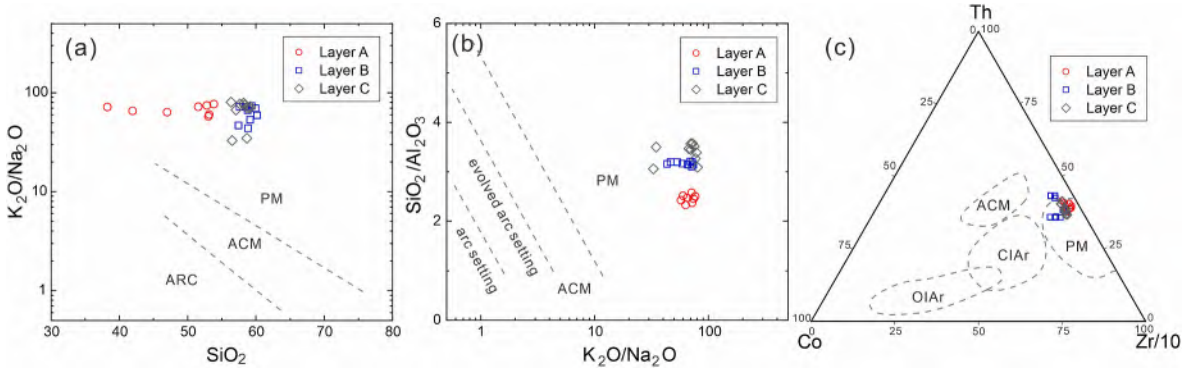

Fig. 12. Parent-rock interpretations by major and trace element geochemical data. (a) TiO_2 vs. Zr (modified from Hayashi et al. (1997)); (b) TiO_2 vs. Al_2O_3 (modified from Schieber (1992)); (c) Th vs. Sc (modified from Totten et al. (2000)); (d) Th/Sc vs. Zr/Sc (after McLennan et al. (1993)); (e) V–Ni–Th*10 ternary diagram (after Bracciali et al. (2007)); (f) SiO_2/10-K_2O + Na_2O–TiO_2+MgO + FeO* ternary diagram (modified from Kroonenberg (1994)); the PCT therein is a primary igneous source composition line, using the gabbro to granite averages. The UCC and PAAS data are from Rudnick and Gao (2014), and Taylor and McLennan (1985), respectively.

Fig. 13. Tectonic setting interpretations by major and trace element geochemical data. (a) K_2O/Na_2O vs. SiO_2 (modified from Roser and Korsch (1986)); (b) SiO_2/Al_2O_3 vs. K_2O/Na_2O (modified from Roser and Korsch (1986)); (c) Th–Co–Zr/10 ternary diagram (after Bhatia and Crook (1986)). OIAr: Oceanic island arc; CIAr: Continental island arc; ACM: Active continental margin; PM: Passive margin; ARC: Oceanic island arc.

thin mixed sedimentary rocks set apart the lower and upper thick dolomite rocks. Especially, the unconformity at the base of the middle Dengying Formation occurs widely throughout the western Yangtze Block, which represents a hiatus between the lower and middle Dengying Formation (Zhu et al., 2003, 2007). The duration of the unconformity could be very short, ca. 1 Myr or less (Gu et al., 2021), and its origin remains controversial. A view considered that it was formed due to a tectonic uplift event, such as the Tongwan movement (Yang et al.,

Table 1
Representative element ratios and proxy values of the analyzed samples.

Beds	Samples	SiO_2/Al_2O_3	CIA	ICV	Th/Sc	Th/U	U/Al	Mo/Al	∑REEs	Eu/Eu*	$Gd_{(n)}/Yb_{(n)}$
Layer A	GPS808-1	2.42	71.8	0.76	1.08	4.17	0.41	0.05	923	0.56	2.38
	GPS808-2	2.57	71.6	1.88	0.82	3.30	0.45	0.05	593	0.57	1.99
	GPS808-3	2.47	71.6	1.45	1.01	4.04	0.38	0.07	714	0.52	2.90
	GPS808-4	2.51	71.7	0.80	1.24	4.15	0.43	0.06	922	0.58	2.57
	GPS808-5	2.45	72.1	0.78	1.25	3.72	0.41	0.10	792	0.56	2.44
	GPS808-6	2.50	71.8	0.82	1.16	3.59	0.45	0.06	874	0.60	2.32
	GPS808-7	2.33	71.5	1.01	1.06	3.55	0.46	0.08	957	0.61	2.70
	GPS808-8	2.37	71.6	0.81	1.10	3.59	0.45	0.10	1071	0.59	2.61
Layer B	GPS808-9	3.14	70.8	0.72	1.03	1.08	1.49	0.20	319	0.59	1.26
	GPS808-10	3.17	70.9	0.70	1.05	1.10	1.42	0.11	304	0.57	1.06
	GPS808-11	3.16	71.1	0.74	1.32	1.63	1.17	0.16	263	0.61	1.14
	GPS808-12	3.19	71.5	0.75	1.28	1.67	1.12	0.15	258	0.61	1.23
	GPS808-13	3.19	71.4	0.76	1.17	1.50	1.23	0.14	270	0.58	1.27
	GPS808-14	3.21	71.0	0.73	0.99	1.16	1.30	0.12	293	0.58	1.12
	GPS808-15	3.14	71.0	0.72	0.94	1.32	1.06	0.18	290	0.59	1.35
	GPS808-16	3.10	71.5	0.75	1.00	1.33	1.15	0.20	313	0.59	1.40
	GPS808-17	3.20	70.3	0.88	0.98	1.65	0.90	0.15	258	0.62	1.18
	GPS808-18	3.19	71.2	0.82	1.00	1.67	0.87	0.16	255	0.59	1.34
Layer C	GPS808-19	3.39	67.2	0.74	1.16	0.63	2.91	0.42	278	0.58	1.16
	GPS808-20	3.52	68.0	0.73	1.01	0.58	2.54	0.32	219	0.62	1.05
	GPS808-21	3.57	67.7	0.71	1.04	0.59	2.44	0.35	186	0.61	1.01
	GPS808-22	3.57	67.7	0.72	1.19	0.66	2.57	0.35	220	0.60	1.16
	GPS808-23	3.50	66.6	0.74	1.01	0.58	2.66	0.30	282	0.60	1.51
	GPS808-24	3.47	67.5	0.79	1.19	0.65	2.29	0.43	211	0.58	1.15
	GPS808-25	3.45	68.8	0.72	0.94	0.54	2.54	0.27	252	0.57	1.20
	GPS808-26	3.09	69.7	0.75	0.97	0.56	2.59	0.37	352	0.52	1.44
	GPS808-27	3.27	69.6	0.74	0.98	0.58	2.45	0.24	305	0.55	1.36
	GPS808-28	3.06	68.6	0.74	0.99	0.55	2.69	0.39	379	0.55	1.49

$CIA = Al_2O_3/(Al_2O_3 + K_2O + Na_2O + CaO^*) \times 100$ (all variables represent the molar amounts of major-element oxide, and the CaO* represents its fraction in silicate minerals only); $ICV = (Fe_2O_3 + K_2O + Na_2O + CaO + MgO + MnO + TiO_2)/Al_2O_3$. $Eu/Eu^* = Eu_{(n)}/(Sm_{(n)} \times Gd_{(n)})^{1/2}$. The unit of ∑REEs values is ppm. The units of the U/Al and Mo/Al ratios are ppm/(wt.%).

2017b; He et al., 2023), and another view regarded it as being formed due to the sea-level change (Zhu et al., 2007; Cui et al., 2019; Deng et al., 2020; Gu et al., 2021). We preferred the sea-level change view in that there is no distinguishable angle unconformity recognized in the seismic data (Gu et al., 2021) and the relative fall of sea-level can produce regression and related short-lived hiatus as well as erosional unconformity.

Focusing on the mixed sedimentary succession above the unconformity, although the Member 3 is only ca. 1 m thick at the Laoya section, it shows a complete transgressive and deepening sequence, which can be correlated with other localities in the Yangtze Block (Zhu et al., 2003, 2007; Yang et al., 2017a; Cui et al., 2019; Deng et al., 2020). The trace elemental indices (Table 1) and the diagram of U/Al versus Mo/Al (Fig. 11) related to the redox conditions show a progressive anoxic trend from base to top, indicating that a widespread transgressive event occurred across the Yangtze Block during the Dengying Member 3 depositional time. This event resulted in the formation of a mixed sedimentary succession as sea water reached emergent continent basement. The sea level rise was a regional event in the Yangtze Block. For some localities, the mixed sedimentary successions are up to 100 m with the development of thin bedded cherts.

In summary, the overall Dengying Formation (ca. 551-539 Ma) in the western Yangtze Block was deposited in a passive margin setting. After the deposition of the lower Dengying Formation (ca. 551-548 Ma), a large sea-level fall occurred throughout the western Yangtze Block resulting in the formation of regional erosional unconformity (ca. 1 Myr or less). Immediately followed by an extensive transgression, a mixed sedimentary succession interbedded with thin volcanic ash layers formed comprising the middle Dengying Formation (ca. 547-546 Ma), indicating a progressive deepening anoxic event. In this process, sediments were derived from nearby felsic-intermediate source terranes and experienced moderate weathering alternation. Finally, this transgressive event led to a landward deposition of the Member 4 (ca. 546-539 Ma) compared to the Member 2. The mixed lithostratigraphic succession with a minor volcanic event in the Yangtze Block can be well correlated with other continents around the world.

6. Conclusions

The terminal Ediacaran Dengying Formation is widely distributed in the western Yangtze Block, South China, characterized by thick dolomites deposited in a shallow-water setting. A distinctive succession of mixed sedimentary rocks occurs in the middle Dengying Formation, however, the absolute age, tectonic and sedimentary environments remain controversial. In this paper, we integrated mineralogy, whole-rock geochemistry, zircon U–Pb-Hf-O isotopic element analyses for a mudstone succession (ca. 1 m thick) from the middle Dengying Formation at the Laoya section in order to constrain the depositional age of the middle Dengying Formation and to unravel its tectonic and sedimentary settings.

(1) We obtained a new SHRIMP zircon U–Pb age of 547.3 ± 4.8 Ma from a volcanic ash within a mudstone succession in the middle Dengying Formation, which is consistent with previously published ages in the middle Dengying Formation or its equivalents in the Yangtze Block and in other continents worldwide.
(2) The stratigraphic correlation and the $\delta^{13}C$ isotopic excursion for the middle Dengying Formation and its equivalents between South China, Oman and Namibia is approximately identical. This consistency of geochronological results and chemostratigraphic trends indicates that the Late Ediacaran $\delta^{13}C$ fluctuations reflect global synchronous variations in seawater chemistry.
(3) Mineralogical, geochemical and Lu-Hf-O isotopic analyses for the Member 3 mudstones indicate that they are dominated by high compositionally mature sediments under an increasing anoxic setting. These sediments were derived from felsic-intermediate rocks with moderate weathering intensity.

(4) Regional geological analysis combining with the geochemical data reveal that the Member 3 mudstone succession was accumulated in a passive margin setting, reflecting an extensive and short-lived transgression event.

Credit author statement

Zhidong Gu: Conceptualization, Methodology, Formal analysis (field investigation, stratigraphic correlation, U–Pb–O-Hf isotopic element analyses), Writing-Original draft, Project administration, Funding acquisition. Xing Jian: Methodology, Formal analysis (mineralogy, geochemical element analyses), Writing-Original draft. Guixia Liu: Formal analysis (stratigraphic correlation).

Declaration of competing interest

The authors declare that they have no known competing financial interests or personal relationships that could have appeared to influence the work reported in this paper.

Data availability

Data will be made available on request.

Acknowledgements

We are grateful to Baomin Zhang, Jinjiang Liu, Shenghui Deng, Hua Jiang, Xiufen Zhai and Hui Zhou, from Research Institute of Petroleum Exploration and Development, PetroChina, for their help during the fieldwork and useful discussions. We would like to thank Shiwen Xie, Wei Zhang, Xiaochao Che and Peizhi Wang, from the Beijing SHRIMP Center, Institute of Geology, Chinese Academy of Geological Sciences, for their assistance during U–Pb–O isotopic element measurements. We sincerely acknowledge Section Editor Prof Salvatore Critelli, from Università della Calabria, Italy, for his encouragement and valuable comments. We would like to thank Dr Ping Gao, from China University of Geosciences (Beijing), for his insightful comments that have largely improved our manuscript. This study was supported by the National Petroleum Project of China (no. 2016ZX05004005-001) and the Science and Technology Project of PetroChina (2023ZZ0201, 2021DJ0501, 2022KT0101, and KT2020-01-03).

Appendix A. Supplementary data

Supplementary data to this article can be found online at https://doi.org/10.1016/j.marpetgeo.2023.106509.

References

Bhatia, M.R., Crook, K.A., 1986. Trace element characteristics of graywackes and tectonic setting discrimination of sedimentary basins. Contrib. Mineral. Petrol. 92, 181–193.

Black, L.P., Kamo, S.L., Allen, C.M., Davis, D.W., Aleinikoff, J.N., Valley, J.W., Mundil, R., Campbell, I.H., Korsch, R.J., Williams, I.S., Foudoulis, C., 2004. Improved $^{206}Pb/^{238}U$ microprobe geochronology by the monitoring of a trace-element-related matrix effect; SHRIMP, ID-TIMS, ELA-ICP-MS and oxygen isotope documentation for a series of zircon standards. Chem. Geol. 205, 115–140.

Bowring, S.A., Grotzinger, J.P., Condon, D.J., Ramezani, J., Newall, M.J., Allen, P.A., 2007. Geochronologic constraints on the chronostratigraphic framework of the neoproterozoic huqf supergroup, sultanate of Oman. Am. J. Sci. 307, 1097–1145.

Bracciali, L., Marroni, M., Luca, P., Sergio, R., 2007. Geochemistry and petrography of Western Tethys Cretaceous sedimentary covers (Corsica and Northern Apennines): from source areas to configuration of margins. In: Sedimentary Provenance and Petrogenesis: Perspectives from Petrography and Geochemistry. GSA Special Papers.

Cao, R., Tang, T., Xue, Y., Yu, C., Yin, L., Zhao, W., 1989. Research on Sinian strata with ore deposits in the Yangzi (Yangtze) region, China. In: Nanjing Institute of Geology and Palaeontology, Academia Sinica. Upper Precambrian of the Yangzi (Yangtze) Region, China. Nanjing University Press, Nanjing, pp. 1–94 (in Chinese with English abstract).

Carpentier, M., Weis, D., Chauvel, C., 2013. Large U loss during weathering of upper continental crust: the sedimentary record. Chem. Geol. 340, 91–104.

Cawood, P.A., Zhao, G.C., Yao, J.L., Wang, W., Xu, Y.J., Wang, Y.J., 2018. Reconstructing South China in phanerozoic and precambrian supercontinents. Earth Sci. Rev. 186, 173–194.

Chen, J., Yang, R., 2010. Analysis on REE geochemical characteristics of three types of REE-rich soil in Guizhou Province, China. J. Rare Earths 28, 517–522.

Chen, Z., Zhou, C.M., Xiao, S.H., Wang, W., Guan, C.G., Hua, H., Yuan, X.L., 2014. New Ediacara fossils preserved in marine limestone and their ecological implications. Sci. Rep. 4, 4180.

Cocks, L.R.M., Torsvik, T.H., 2013. The dynamic evolution of the Palaeozoic geography of eastern Asia. Earth Sci. Rev. 117, 40–79.

Compston, W., Williams, I.S., Kirschvink, J.L., Zhang, Z.C., Guogan, M.A., 1992. Zircon U-Pb ages for the early cambrian time-scale. J. Geol. Soc. 149, 171–184.

Condon, D., Zhu, M.Y., Bowring, S., Wang, W., Yang, A.H., Jin, Y.G., 2005. U-Pb ages from the neoproterozoic Doushantuo Formation, China. Science 308, 95–98.

Cox, R., Lowe, D.R., Cullers, R.L., 1995. The influence of sediment recycling and basement composition on evolution of mudrock chemistry in the southwestern United States. Geochem. Cosmochim. Acta 59 (14), 2919–2940.

Cui, H., Kaufman, A.J., Xiao, S., Peek, S., Cao, H., Min, X., Cai, Y., Siegel, Z., Liu, X.M., Peng, Y., Schiffbauer, J.D., Martin, A.J., 2016. Environmental context for the terminal Ediacaran biomineralization of animals. Geobiology 14, 344–363.

Cui, H., Xiao, S., Cai, Y.P., Peek, S., Plummer, R.E., Kaufman, A.J., 2019. Sedimentology and chemostratigraphy of the terminal ediacaran Dengying Formation at the gaojiashan section, South China. Geol. Mag. 156 (11), 1924–1948.

Dalziel, I.W.D., 1997. Neoproterozoic-Paleozoic geography and tectonics: review, hypothesis, environmental speculation. GSA Bulletin 109 (1), 16–42.

Deng, S.H., Fang, R., Li, X., Zhang, S.B., Zhang, B.M., Lu, Y.Z., 2015. Subdivision and correlation of the sinian (ediacaran) system in the Sichuan Basin and its adjacent area. J. Stratigr. 39 (3), 239–254.

Deng, S.L., Song, J.M., Liu, S.G., Luo, P., Li, Z.W., Yang, D., Sun, W., Li, J.X., Yu, J.J., Li, L.J., 2020. Mixed sedimentary characteristics of the third member of Dengying Formation, Sichuan Basin, and its geological significance. Acta Sedimentol. Sin. 38 (3), 598–609 (In Chinese with English abstract).

Ding, L., Zhang, L., Li, Y., Dong, J., 1992. The Study of the Late Sinian-Early Cambrian Biota from the Northern Margin of Yangtze Platform. Scientific and Technical Documents Publishing House, Beijing, pp. 1–156 (In Chinese with English abstract).

Domeier, M., 2018. Early Paleozoic tectonics of Asia: towards a full-plate model. Geosci. Front. 9, 789–862.

Duda, J.P., Zhu, M.Y., Reitner, J., 2016. Depositional dynamics of a bituminous carbonate facies in a tectonically induced intra-platform basin: the Shibantan Member (Dengying Formation, Ediacaran Period). Carbonates Evaporites 31, 87–99.

Feng, M.Y., Wu, P.C., Yan, X.R., Liu, X.H., Li, N.X., Wu, Y., Chen, D., He, J.G., 2017. Geochemistry and significance of shale in the third member of the precambrian Dengying Formation, ebian of southwestern sichuan. Bull. China Soc. Mineral Petrol. Geochem. 36 (3), 493–501 (In Chinese with English abstract).

Fu, H., Jian, X., Liang, H., Zhang, W., Shen, X., Wang, L., 2022. Tectonic and climatic forcing of chemical weathering intensity in the northeastern Tibetan Plateau since the middle Miocene. Catena 208, 105785.

Gamper, A., Struck, U., Ohnemueller, F., Heubeck, C., Hohl, S., 2015. Chemo- and biostratigraphy of the Gaojiashan section (northern Yangtze platform, South China): a new Pc-C boundary section. Fossil Record 18, 105–117.

Grotzinger, J.P., Bowring, S.A., Saylor, B.Z., Kaufman, A.J., 1995. Biostratigraphic and geochronologic constraints on early animal evolution. Science 270, 598–604.

Gu, Z.D., Zhang, W., Yuan, M., 2014. Zircon SHRIMP U-Pb dating of basal granite and its geological significance in Weiyuan area of Sichuan Basin. Chinese Journal of Geology 49 (1), 202–213 (in Chinese with English abstract).

Gu, Z.D., Lonergan, L., Zhai, X.F., Zhang, B.M., Lu, W.H., 2021. The formation of the Sichuan Basin, South China, during the late ediacaran to early cambrian. Basin Res. 33, 12559.

Gu, Z.D., Jiang, H., Fu, L., Zhang, B.M., Zhai, X.F., Liu, G.X., Li, Q.F., 2023. Ediacaran stratigraphy and paleogeography in the north Yangtze block, South China. Sediment. Geol. 444, 106314.

Hayashi, K.I., Fujisawa, H., Holland, H.D., Ohmoto, H., 1997. Geochemistry of ~ 1.9 Ga sedimentary rocks from northeastern Labrador, Canada. Geochem. Cosmochim. Acta 61 (19), 4115–4137.

He, R.W., Sun, W., Li, Z.Q., Deng, B., Miao, R.L., Zhang, C.J., Tian, T.Z., Lu, P.D., 2023. Sedimentary characteristics and geological significance of the third member of Sinian Dengying Formation in Liuwanxiang area, northern Sichuan. J. Chengdu Univ. Technol. (Sci. Technol. Ed.) 50 (1), 50–64 (In Chinese with English abstract).

Herron, M.M., 1988. Geochemical classification of terrigenous sands and shales from core or log data. J. Sediment. Res. 58 (5), 820–829.

Hu, M.Y., Gao, D., Wei, G.Q., Yang, W., Xie, W.R., 2018. Sequence stratigraphy and facies architecture of a mound-shoal-dominated dolomite reservoir in the late Ediacaran Dengying Formation, central Sichuan Basin, SW China. Geol. J. 1–19.

Jian, X., Guan, P., Zhang, W., Feng, F., 2013. Geochemistry of Mesozoic and Cenozoic sediments in the northern Qaidam basin, northeastern Tibetan Plateau: implications for provenance and weathering. Chem. Geol. 360, 74–88.

Jiang, G.Q., Kennedy, M.J., Christie-Blick, N., 2003. Stable isotopic evidence for methane seeps in Neoproterozoic postglacial cap carbonates. Nature 426, 822–826.

Jiang, G.Q., Kaufman, A.J., Christie-Blick, N., Zhang, S.H., Wu, H.C., 2007. Carbon isotope variability across the Ediacaran Yangtze platform in South China: implications for a large surface-to-deep ocean $\delta^{13}C$ gradient. Earth Planet Sci. Lett. 261, 303–320.

Jiang, G.Q., Shi, X.Y., Zhang, S.H., Wang, Y., Xiao, S.H., 2011. Stratigraphy and paleogeography of the ediacaran Doushantuo Formation (ca. 635-551 Ma) in South China. Gondwana Res. 19, 831–849.

Jin, C., Li, C., Algeo, T.J., Wang, G., Shi, W., Cheng, M., Zhang, Z., Wang, H., Li, D., Wang, W., 2021. Spatial heterogeneity of redox-sensitive trace metal enrichments in upper Ediacaran anoxic black shales. J. Geol. Soc. 178 (5).
Jing, X.Q., Yang, Z.Y., Tong, Y.B., Han, Z.R., 2015. A revised paleomagnetic pole from the mid-Neoproterozoic Liantuo Formation in the Yangtze block and its paleogeographic implications. Precambrian Res. 268, 194–211.
Knoll, A.H., Walter, M.R., Narbonne, G.M., Christie-Blick, N., 2004. A new period for the geologic time scale. Science 305, 621–622.
Knoll, A.H., Walter, M.R., Narbonne, G.M., Christie-Blick, N., 2006. The Ediacaran Period: a new addition to the geologic time scale. Lethaia 39, 13–30.
Kroonenberg, S.B., 1994. Effects of provenance, sorting and weathering on the geochemistry of fluvial sands from different tectonic and climatic environments. Proceedings of the 29th international geological congress, Part A 69–81.
Lan, C., Xu, Z., Yang, D., Yang, W., Lu, C., Chen, H., Li, P., Wang, Y., Zou, H., 2022. Stratigraphy and depositional evolution of the terminal Ediacaran platform in the central to northern Sichuan Basin, Southwest China. Palaeogeogr. Palaeoclimatol. Palaeoecol. 601, 111142.
Li, J.Y., Wang, X.L., Gu, Z.D., 2018. Early neoproterozoic arc magmatism of the tongmuliang Group on the northwestern margin of the Yangtze block: implications for Rodinia assembly. Precambrian Res. 309, 181–197.
Li, J.Y., Tang, M., Lee, C.A., Wang, X.L., Gu, Z.D., Xia, X.P., Wang, D., Du, D.H., Li, L.S., 2021. Rapid endogenic rock recycling in magmatic arcs. Nat. Commun. 12, 3533.
Linnemann, U., Ovtcharova, M., Schaltegger, U., Gärtner, A., Hautmann, M., Geyer, G., Vickers-Rich, P., Rich, T., Plessen, B., Hofmann, M., Zieger, J., Krause, R., Kriesfeld, L., Smith, J., 2019. New high-resolution age data from the Ediacaran-Cambrian boundary indicate rapid, ecologically driven onset of the Cambrian explosion. Terra. Nova 31 (1), 49–58.
Liu, S., Yang, Y., Deng, B., Zhong, Y., Wen, L., Sun, W., Li, Z., Jansa, L., Li, J., Song, J., Zhang, X., Peng, H., 2021. Tectonic evolution of the Sichuan basin, southwest China. Earth Sci. Rev. 213, 103470.
McDonough, W.F., Sun, S.S., 1995. The composition of the Earth. Chem. Geol. 120 (3–4), 223–253.
McLennan, S.M., 1989. Rare earth elements in sedimentary rocks: influence of provenance and sedimentary processes. Rev. Mineral. 21, 169–200.
McLennan, S.M., Hemming, S., McDaniel, D.K., Hanson, G.N., 1993. Geochemical Approaches to Sedimentation, Provenance, and Tectonics. Special Papers-Geological Society of America, p. 21.
Merdith, A.S., Collins, A.S., Williams, S.E., Pisarevsky, S., Foden, J.D., Archibald, D.B., Blades, M.L., Alessio, B.L., Armistead, S., Plavsa, D., Clark, C., Müller, R.D., 2017. A full-plate global reconstruction of the Neoproterozoic. Gondwana Res. 50, 84–134.
Nesbitt, H.W., Young, G.M., 1982. Early Proterozoic climates and plate motions inferred from major element chemistry of lutites. Nature 299, 715–717.
Nesbitt, H.W., Fedo, C.M., Young, G.M., 1997. Quartz and feldspar stability, steady and non-steady-state weathering, and petrogenesis of siliciclastic sands and muds. J. Geol. 105, 173–191.
Qi, L., Xu, Y., Cawood, P.A., Du, Y., 2018. Reconstructing cryogenian to ediacaran successions and paleogeography of the SouthSouth China block. Precambrian Res. 314, 452–467.
Roser, B.P., 2000. Whole-rock geochemical studies of clastic sedimentary suites. Member Geological Society Japan 57, 73–89.
Roser, B.P., Korsch, R.J., 1986. Determination of tectonic setting of sandstone-mudstone suites using SiO_2 content and K_2O/Na_2O ratio. J. Geol. 94 (5), 635–650.
Roser, B.P., Korsch, R.J., 1988. Provenance signatures of sandstone-mudstone suites determined using discriminant function analysis of major-element data. Chem. Geol. 67, 119–139.
Rudnick, R.L., Gao, S., 2014. Composition of the continental crust. The crust 3, 1–51.
Schieber, J., 1992. A combined petrographical—geochemical provenance study of the Newland Formation, Mid-Proterozoic of Montana. Geol. Mag. 129 (2), 223–237.
Song, Z., Liu, C., Han, G., Wang, Z., Zhu, Z., Yang, C., 2006. Enrichment and release of rare earth elements during weathering of sedimentary rocks in Wujiang Catchments, Southwest China. J. Rare Earths 24 (4), 491–496.
Taylor, S.R., McLennan, S.M., 1985. The Continental Crust: its Composition and Evolution Geoscience Texts, vol. 312. Blackwell Scientific Publications.
Totten, M.W., Hanan, M.A., Weaver, B.L., 2000. Beyond whole-rock geochemistry of shales: the importance of assessing mineralogic controls for revealing tectonic discriminants of multiple sediment sources for the Ouachita Mountain flysch deposits. Geol. Soc. Am. Bull. 112 (7), 1012–1022.
Vernhet, E., Heubeck, C., Zhu, M.Y., Zhang, J.M., 2006. Large-scale slope instability at the southern margin of the Ediacaran Yangtze platform (Hunan province, central China). Precambrian Res. 148, 32–44.
Wang, J., Li, Z.X., 2003. History of Neoproterozoic rift basins in South China: implications for Rodinia break-up. Precambrian Res. 122, 141–158.
Wei, G.Q., Yang, W., Du, J.H., Xu, C.C., Zou, C.N., Xie, W.R., Zeng, F.Y., Wu, S.J., 2015. Geological features of sinian-early cambrian intracratonic rift of the Sichuan Basin. Nat. Gas. Ind. B 2, 37–48.
Woodhead, J.D., Hergt, J.M., 2005. A preliminary appraisal of seven natural zircon reference materials for in situ Hf isotope determination. Geostand. Geoanal. Res. 29 (2), 183–195.
Xiao, Q., She, Z., Wang, G., Li, Y., Ouyang, G., Cao, K., Mason, R., Du, Y., 2020. Terminal ediacaran carbonate tempestites in the eastern Yangtze Gorges area, South China. Palaeogeogr. Palaeoclimatol. Palaeoecol. 547, 109681.
Xing, F.C., Hou, M.C., Lin, L.B., Xu, S.L., Hu, H.R., 2015. The records and its dynamic genesis discussion of tectonic movement during the Late Sinian and the Early Cambrian of Sichuan Basin. Earth Sci. Front. 22 (1), 115–125 (in Chinese with English abstract).
Xu, Z., Han, G., 2009. Rare earth elements (REE) of dissolved and suspended loads in the Xijiang River, South China. Appl. Geochem. 24 (9), 1803–1816.
Xu, C.C., Shen, P., Yang, Y.M., Zhao, L.Z., Luo, B., Wen, L., Cheng, G., Ran, Q., Zhong, Y., Peng, H.L., 2020. New understandings and potential of Sinian-Lower Paleozoic natural gas exploration in the central Sichuan paleo-uplift of the Sichuan Basin. Nat. Gas. Ind. 40 (7), 1–9 (in Chinese with English abstract).
Xue, R.S., Cao, R.J., Tang, T.F., Yin, L.M., Yu, C.L., 2001. The Sinian stratigraphic sequence of the Yangtze region and correlation to the Late Precambrian strata of North China. J. Stratigr. 25 (3), 207–234 (in Chinese with English abstract).
Yang, Z., Sun, Z., Yang, T., Pei, J., 2004. A long connection (750-380 Ma) between South China and Australia: paleomagnetic constraints. Earth Planet Sci. Lett. 220, 423–434.
Yang, Y., Huang, X.P., Zhang, J., Yang, G., Song, J.R., Song, L.K., Hong, H.T., Tan, X.C., Wen, L., 2014. Features and geologic significances of the top Sinian karst landform before the Cambrian deposition in the Sichuan Basin. Nat. Gas. Ind. 34 (3), 38–43 (in Chinese with English abstract).
Yang, C., Li, X.H., Zhu, M.Y., Condon, D.J., 2017a. SIMS U-Pb zircon geochronological constraints on upper Ediacaran stratigraphic correlations, South China. Geol. Mag. 154 (6), 1202–1216.
Yang, C., Zhu, M.Y., Condon, D.J., Li, X.H., 2017b. Geochronological constraints on stratigraphic correlation and oceanic oxygenation in Ediacaran-Cambrian transition in South China. J. Asian Earth Sci. 140, 75–81.
Yao, W.H., Li, Z.X., Li, W.X., Li, X.H., Yang, J.H., 2014. From Rodinia to Gondwana-land: a tale of detrital zircon provenance analyses from the southern NanhuaBasin, South China. Am. J. Sci. 314, 278–313.
Ye, M.F., Li, X.H., Li, W.X., Liu, Y., Li, Z.X., 2007. SHRIMP zircon U-Pb geochronological and whole-rock geochemical evidence for an early Neoproterozoic Sibaoan magmatic arc along the southeastern margin of the Yangtze Block. Gondwana Res. 12, 144–156.
Zhai, L., Wu, C., Ye, Y., Zhang, S., Wang, Y., 2018. Fluctuations in chemical weathering on the Yangtze Block during the Ediacaran–Cambrian transition: implications for paleoclimatic conditions and the marine carbon cycle. Palaeogeogr. Palaeoclimatol. Palaeoecol. 490, 280–292.
Zhao, G.C., Cawood, P.A., 2012. Precambrian geology of China. Precambrian Res. 222–223, 13–54.
Zhao, Z., Xing, Y., Ma, G., Chen, Y., 1985. Biostratigraphy of the Yangtze Gorges Area: (1) Sinian. Geological Publishing House, Beijing, pp. 1–143 (in Chinese with English abstract).
Zhou, C.M., Xiao, S.H., 2007. Ediacaran $\delta^{13}C$ chemostratigraphy of South China. Chem. Geol. 237, 89–108.
Zhou, Z., Wang, X.Z., Yin, G., Yuan, S.S., Zeng, S.J., 2016. Characteristics and genesis of the (sinian) Dengying Formation reservoir in central sichuan, China. J. Nat. Gas Sci. Eng. 29, 311–321.
Zhou, H., Li, W., Zhang, B.M., Liu, J.J., Deng, S.H., Zhang, S.B., Shan, X.Q., Zhang, J., Wang, X.B., Jiang, H., 2017. Formation and evolution of intraplatform basin from the late Sinian to early Cambrian in Sichuan Basin, China. Petroleum Research 2, 41–53.
Zhou, M.Z., Luo, T.Y., Huff, W.D., Yang, Z.Q., Zhou, G.H., Gan, T., Yang, H., Zhang, D., 2018. Timing the termination of the Doushantuo negative carbon isotope excursion: evidence from U-Pb ages from the Dengying and Liuchapo formations, South China. Sci. Bull. 63, 1431–1438.
Zhou, C.M., Yuan, X.L., Xiao, S.H., Chen, Z., Hua, H., 2019. Ediacaran integrative stratigraphy and timescale of China. Sci. China Earth Sci. 62 (1), 7–24.
Zhu, M.Y., Zhang, J.M., Michael, S., Yang, A.H., Li, G.X., Erdtmann, B.D., 2003. Sinian-Cambrian stratigraphic framework for shallow- to deep-water environments of the Yangtze Platform: an integrated approach. Prog. Nat. Sci. 13 (12), 951–960.
Zhu, M.Y., Zhang, J.M., Yang, A.H., 2007. Integrated ediacaran (sinian) chronostratigraphy of South China. Palaeogeogr. Palaeoclimatol. Palaeoecol. 254, 7–61.
Zi, J.P., Jia, D., Wei, G.Q., Yang, Z.Y., Zhang, Y., Hu, J., Shen, S.X., 2017. LA-ICP-MS U-Pb zircon ages of volcaniclastic beds of the third Member of the Sinian (Ediacaran) Dengying Formation in Leshan, Sichuan, and a discussion on the rift evolution in the Basin. Geol. Rev. 63 (4), 1041–1049 (In Chinese with English abstract).
Zou, C.N., Du, J.H., Xu, C.C., Wang, Z.C., Zhang, B.M., Wei, G.Q., Wang, T.S., Yao, G.S., Deng, S.H., Liu, J.J., Zhou, H., Xu, A.N., Yang, Z., Jiang, H., Gu, Z.D., 2014. Formation, distribution, resource potential, and discovery of Sinian-Cambrian giant gas field, SichuanBasin, SW China. Petrol. Explor. Dev. 41 (3), 306–325.